

Controlling the CO adsorption on Pt clusters by dopant induced electronic structure modification

Piero Ferrari,^[a] Luis M. Molina,^{*[b]} Vladimir E. Kaydashev,^[a] Julio A. Alonso,^[b] Peter Lievens,^[a] and Ewald Janssens,^{*[a]}

Abstract: A major drawback of state-of-the-art proton exchange membrane fuel cells is the CO poisoning of platinum catalysts. It is known that CO poisoning is reduced if platinum alloys are used, but the underlying mechanism therefore is still under debate. We study the influence of dopant atoms on the CO adsorption on small platinum clusters using mass spectrometry experiments and density functional theory calculations. A significant reduction in the reactivity for Nb and Mo doped clusters is attributed to electron transfer from those highly coordinated dopants to the Pt atoms and the concomitant lower CO binding energies. On the other hand Sn and Ag dopants have a lower Pt coordination and have a limited effect on the CO adsorption. Analysis of the density of states demonstrates a correlation of dopant induced changes in the electronic structure with the enhanced tolerance to CO poisoning.

The development of efficient fuel cells is a promising strategy to diminish the dependence on fossil fuel by making use of environmentally friendly energy sources.^[1] Proton exchange membrane fuel cells (PEMFCs) are highly susceptible to CO poisoning of the platinum catalyst.^[2] CO molecules, present as trace components in the fuel, preferentially adsorb on Pt nanoparticles, thereby blocking the active sites and degrading the cell's performance. Several Pt alloys, such as Pt–X (X = Sn, Ru, Mo, Nb, W, Ag, and Ni), are known for an enhanced tolerance to the CO poisoning and thus improve the performance of the fuel cell.^[3–7] The physical mechanism responsible for the tolerance has been extensively studied and is ascribed to an alteration of the local electronic structure at the reaction site upon alloying and/or to a bi-functional mechanism, in which OH groups adsorbed on the alloying agent interact with CO and form CO₂ and H₂, which are released from the catalyst, regenerating the active sites.^[3]

The interaction of transition metal surfaces with CO is a complex problem which has been described by three qualitative models: the d-band center model,^[8] the Blyholder model,^[9] and the π - σ model.^[10] In the Blyholder model, the Pt–CO interaction

is described by donation of electron density from the CO 5 σ orbital to empty Pt 5d states and back-donation from occupied Pt 5d states to the CO 2 π^* antibonding orbital. The bottom-line of local electronic structure modifications as explanation for the CO tolerance in Pt–X alloy nanoparticles is that electron transfer from the alloying agent to the empty Pt 5d states reduces the Pt–CO bonding strength.^[11]

Although few-atom platinum clusters in the gas phase differ significantly in size and in environmental conditions from the nanoparticles used in PEMFCs, they can provide a better understanding for the enhanced tolerance to CO poisoning. The CO binding is a local event, which poisons a Pt active site. Clusters in molecular beams are ideal model system for complex processes that depend on local chemistry. Conditions (cluster size, composition, and charge state) are well controlled in a gas phase experiment. In addition, reactions with unknown molecules are excluded if the experiments are performed under high vacuum conditions while the small size of the clusters allows for direct comparison with quantum chemical calculations.^[12,13] For instance, studies on the small Pd₆⁺ cluster identified the Pd₆O₄⁺ oxide as a key intermediate in the catalytic combustion of CO.^[14] Joined experimental and theoretical studies on V_xO_y⁺ clusters elucidated the nature of the active site in the catalytic ethylene oxidation on vanadium oxide,^[15] and experiments on Au₂⁺ clusters demonstrated the activation of methane on Au with subsequent release of ethylene.^[16]

Here we combine mass spectrometric experiments and density functional theory (DFT) calculations to study the influence of dopant atoms on the CO adsorption on small Pt clusters. The size-selected clusters are ideal model systems to investigate how doping modifies the local electronic structure at the active Pt site, thereby altering the CO adsorption strength. At the same time, the experimental high vacuum conditions eliminate the presence of bi-functional mechanisms.^[17]

Cationic doped Pt clusters, XPt_n⁺ (X = Mo, Nb, Sn, and Ag; 13 ≤ n ≤ 23), are produced in a dual-target dual-laser vaporization source. The room temperature clusters are subsequently exposed to CO gas in a low-collision reaction cell and the abundances of the cluster–CO complexes are analyzed by time-of-flight mass spectrometry.^[18] With the used CO pressures ($p_{\text{CO}} = 0$ to 0.05 Pa) up to two CO molecules are adsorbed on the clusters.

A part of the mass spectrum of pure and Nb doped Pt clusters, recorded for a CO pressure of 0.05 Pa in the collision cell, is presented in Figure 1a. For all bare Pt_n⁺ clusters, complexes with one and two CO molecules are formed, while for the doped NbPt_{n-1}⁺ (n = 18–22) clusters the intensity of the complexes with two CO molecules is low. This clearly illustrates the influence of Nb doping on the likelihood for CO adsorption. The molecular beam of clusters interacts with CO in the collision cell and formed complexes are mass analyzed about 100 μ s later, corresponding to the flight time from the cell to the

[a] P. Ferrari, Dr. V. E. Kaydashev*, Prof. Dr. P. Lievens, Prof. Dr. E. Janssens,

Laboratory of Solid State Physics and Magnetism
KU Leuven
Celestijnenlaan 200D, 3001 Leuven (Belgium)
E-mail: ewald.janssens@fys.kuleuven.be

[b] Prof. Dr. L. M. Molina, Prof. Dr. J. A. Alonso
Department of Theoretical, Atomic and Optical Physics
Universidad de Valladolid
Paseo Belén 7, 47011 Valladolid (Spain)
E-mail: lmolina@fta.uva.es

*Current address: Laboratory of Nanomaterials, Southern Federal University, 344090 Rostov-on-Don (Russia)

Supporting information for this article is given via a link at the end of the document.

extraction zone of the mass spectrometer. The influence of the Nb dopant is mainly reflected on the adsorption of the second CO molecule and in the $n=18-22$ size range, which is a consequence of the time scale of the experiment and is explained below.

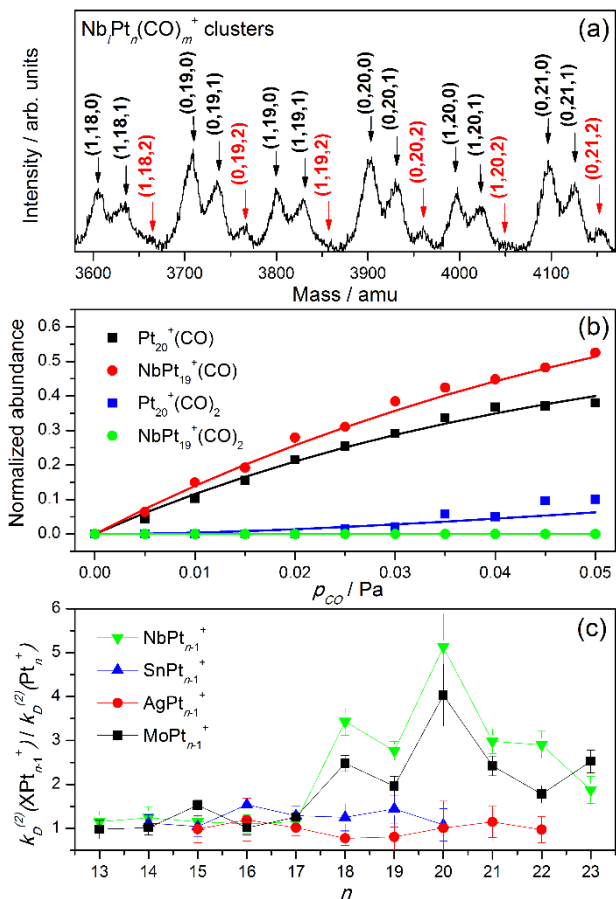
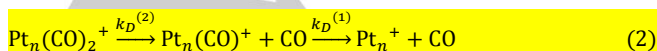
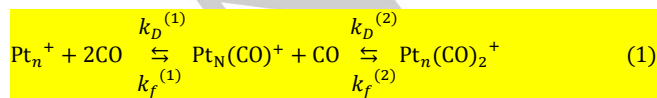


Figure 1. a) Part of the mass spectrum of pure and Nb doped Pt clusters exposed to 0.05 Pa of CO gas. The label (l,n,m) refers to the composition of the complexes $\text{Nb}_l\text{Pt}_n(\text{CO})_m^+$. $(\text{CO})_2$ complexes are marked in red. b) Fit of normalized intensities of (CO) and $(\text{CO})_2$ complexes of Pt_{20}^+ and NbPt_{19}^+ clusters as a function of p_{CO} . c) Size dependence of the ratio of backward reaction coefficients $k_D^{(2)}$ of doped to pure Pt clusters.

Figure 1b illustrates the pressure dependent kinetics data, which reveal an increase in the cluster- (CO) and cluster- $(\text{CO})_2$ complexes with p_{CO} . The formation of cluster-CO complexes can be described by a two-step reaction mechanism, characterized by forward ($k_f^{(1,2)}$) and backward ($k_D^{(1,2)}$) reaction coefficients for adsorption and desorption of the first (1) and second (2) CO molecule.^[18]



where (1) and (2) represent the reaction mechanism for clusters in and after the reaction cell.

The fits presented in Figure 1b show that $k_f^{(1)}$ and $k_f^{(2)}$ can be approximated by hard-sphere collision rates, while the size- and dopant dependent strength of the cluster- $(\text{CO})_{1,2}$ bonds is reflected in the magnitude of $k_D^{(1,2)}$.^[19] A detailed description of this procedure and the validity of the underlying analysis is presented as Supporting Information.

The dependence of the unimolecular dissociation rates on the CO adsorption energies can be simulated with statistical RRKM analysis (see Supporting Information). Desorption rates of the first CO molecule, $k_D^{(1)}$, are found slower than the time scale of the experiment. This explains why size and dopant dependences are only seen in the desorption of the second CO molecule. $k_D^{(2)}$ is significantly higher than $k_D^{(1)}$, because the corresponding clusters are internally heated by adsorption of two instead of one CO molecule. For example, assuming binding energies of 2.4 eV and 2.0 eV for the first and second CO molecule on Pt_{19}^+ (cfr. DFT calculation in Supporting Information), the simulated value of $k_D^{(2)}$ is $6 \cdot 10^3 \text{ s}^{-1}$. A dopant induced reduction of the adsorption energies by 0.4 eV results in an increase of $k_D^{(2)}$ to about 10^7 s^{-1} . Such a high $k_D^{(2)}$ implies dissociation before detection and thus a strong reduction in the measured abundance of the doped cluster- $(\text{CO})_2$ complex.

Because of the finite size of the heat bath, $k_D^{(1,2)}$ strongly depends on the size of the cluster. In a small cluster, with few degrees of freedom, the same CO adsorption energy results in a large temperature increase and thus a high unimolecular dissociation rate.^[17] For example, no cluster- $(\text{CO})_2$ complexes are observed for clusters with less than 17 atoms, since they all dissociate on the time scale of the experiment. Also this observation can be well explained by the RRKM simulations (see Supporting Information).

Figure 1c presents the ratio of the fitted dissociation rates $k_D^{(2)}$ for the doped clusters (with $X = \text{Mo}, \text{Nb}, \text{Sn},$ and Ag) to that of pure Pt clusters as a function of cluster size. Comparing clusters of the same size one can make abstraction of the heat bath effect on the dissociation rates and directly probe the influence of the dopant atom. It is remarkable that $k_D^{(2)}$ is not significantly affected by the substitution of Pt for Sn or Ag dopants ($k_D^{(2)}$ ratio in Figure 1c is around unity), while doping with Mo or Nb leads to a strong increase in $k_D^{(2)}$ for $n > 17$ cluster sizes. This different behavior in terms of CO binding energies will be described further.

Density functional theory (DFT) was used to analyze the chemical bonding of CO with representative Pt_{19}^+ and XPt_{18}^+ ($X = \text{Nb}, \text{Mo}, \text{Ag},$ and Sn) clusters. Simulations were carried out within the projector augmented-wave method as implemented in the GPAW software using a 20 Å cubic cell.^[20,21] The spacing of the real-space 3D grid was set to 0.2 Å and exchange-correlation effects were modelled with the PBE functional.^[22,23] The SCF convergence threshold was set to 10^{-6} eV/e^- . Structure optimization was carried out using the BFGS (Quasi-Newton) algorithm until forces were below 0.01 eV/Å.

The lowest energy structural isomer found for Pt_{19}^+ has an octahedral shape, which has also been predicted computationally for neutral Pt_{19} .^[24] Isomers for XPt_{18}^+ are explored by substituting inequivalent sites of Pt_{19}^+ with the dopant atom, followed by local structural optimization. The

obtained minimum energy structures are shown in Figure 2. Nb and Mo preferentially locate at the cluster core, whereas Ag and Sn occupy an edge site. CO adsorption energies, $E_{\text{ads}} = E_{\text{cluster-CO}} - (E_{\text{cluster}} + E_{\text{CO}})$, are calculated for adsorption of CO to each inequivalent surface site. The largest CO adsorption energies (Table 1), are obtained at edge site (1) for both the Pt_{19}^+ and all XPt_{18}^+ clusters.

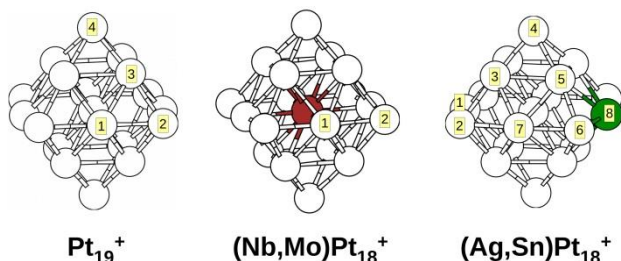


Figure 2. Relaxed structures of Pt_{19}^+ and XPt_{18}^+ clusters ($X = \text{Nb}, \text{Mo}, \text{Ag}, \text{and Sn}$). Dopant atoms are colored in red (Nb, Mo) and green (Ag, Sn). Inequivalent surface sites are numbered.

The CO binds most strongly with pure Pt_{19}^+ ($E_{\text{ads}} = 2.38$ eV), while a much weaker CO binding is found for Nb and Mo doped Pt clusters ($E_{\text{ads}} \approx 1.8$ eV). The values for Ag and Sn doped clusters ($E_{\text{ads}} \approx 2.2$ eV) are close to that of pure Pt. The calculated lower CO binding energy for Nb and Mo doped Pt clusters is in good agreement with the mass spectrometric observations. As shown in the RRKM analysis (see Supporting Information) a reduction in the CO binding energy considerably increases the cluster–CO dissociation rates, which is reflected in lower abundances of cluster–(CO)₂ complexes. The DFT result that Ag and Sn doping only slightly reduces E_{ads} also agrees with the experimental data, since for these dopants no significant change in cluster reactivity was observed.

Table 1. Calculated CO adsorption energies and Bader charges on X in XPt_{18}^+ clusters.

Cluster	$E_{\text{ads}} / \text{eV}$	Bader charge
Pt_{19}^+	-2.38	-
NbPt_{18}^+	-1.81	+1.73
MoPt_{18}^+	-1.83	+1.40
AgPt_{18}^+	-2.26	+0.37
SnPt_{18}^+	-2.21	+0.95

Figure 3 presents an analysis of the clusters' electronic structures. The upper panel shows the total DOS of Pt_{19}^+ and projections into atomic Pt s and d states. As expected, the electronic structure is dominated by valence d states, which form a band ranging from -14 to -7.5 eV. This d band is nearly full, with only 9 empty states from the Fermi level, E_{F} , to the top of the band.

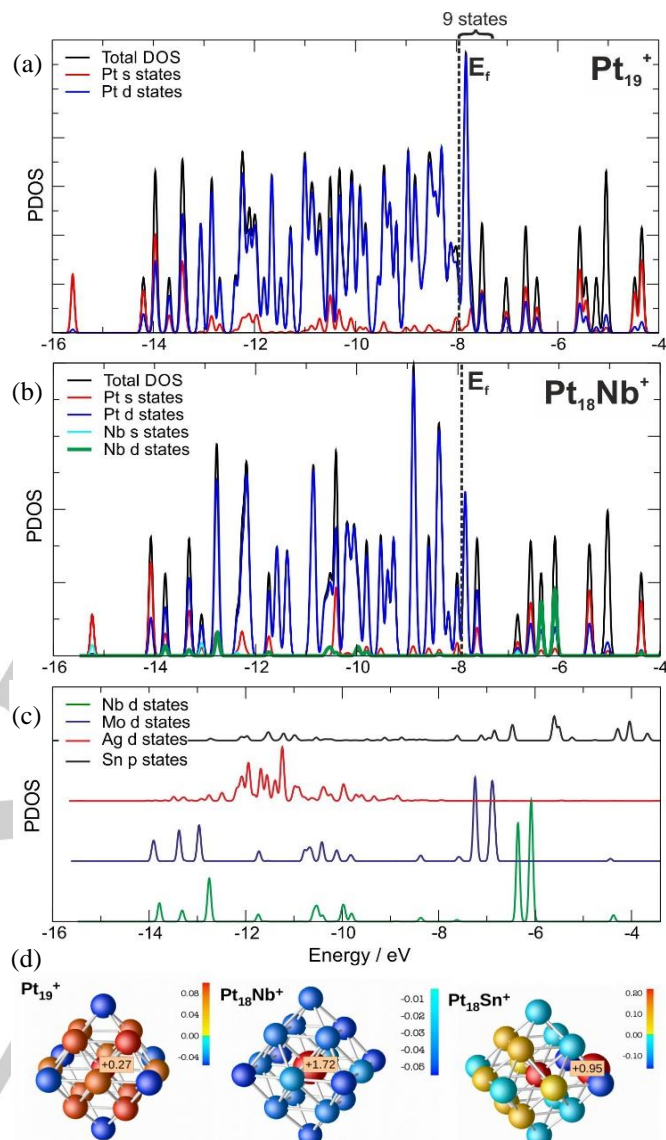


Figure 3. Total and projected densities of states (DOS) for (a) Pt_{19}^+ and (b) NbPt_{18}^+ clusters. (c) Series of projected DOS into the d states of the impurity atom (p states for Sn) for XPt_{18}^+ clusters. (d) Bader charges on Pt_{19}^+ , NbPt_{18}^+ , and SnPt_{18}^+ . Positively (negatively) charged atoms are colored with various shades of red (blue). Labels indicate the value of charges which lie off the scale. The dopant atoms have a larger size.

Figure 3b shows an analogous DOS analysis for NbPt_{18}^+ , including projections on s and d states of Nb. Most of the Nb d states are located above the Fermi level. Nb d electrons are transferred to the Pt d band. Hereby, E_{F} moves up slightly, with only 7 empty states from E_{F} to the top of the valence band. A comparison of the valence occupancy of the different dopants in XPt_{18}^+ is presented in Figure 3c. For heavier dopants the electronegativity difference between dopant and Pt gets smaller and the energy of the dopant's d states decreases. Nb has the largest dopant–host charge transfer, followed by Mo, while most of the Ag d states have energies within the Pt d band. Sn dopants are qualitatively different, as charge transfer takes place from 5p orbitals. The Sn 5p orbitals are located partly inside, and partly outside the Pt d band.

A Bader charge analysis demonstrates dopant induced charge transfer. Figure 3d illustrates that the charge in pure Pt_{19}^+ is distributed over edge-like sites (around +0.09 e at each site) and the central atom (+0.27 e), while there is a very large net positive charge on the central dopant atom in NbPt_{18}^+ (+1.73 e) and all Pt atoms are negatively charged. The Mo dopant in MoPt_{18}^+ has also a large, however slightly lower, net positive charge (see Table 1). In contrast, charge transfer from Ag to the Pt cluster is much smaller. In SnPt_{18}^+ there mainly is charge transfer from the edge located Sn dopant to the neighboring Pt atoms, while other Pt edge sites still have a positive charge. Overall, the Bader charge of the Pt atoms is strongly correlated with CO adsorption energies, with a stronger CO bonding at sites with a more positive charge (see Supporting Information for CO binding energies at different sites). The smaller CO binding energy on NbPt_{18}^+ and MoPt_{18}^+ can thus be rationalized by the large charge transfer from the dopants to all Pt atoms of the clusters. In AgPt_{18}^+ and SnPt_{18}^+ CO preferentially binds on Pt atoms distant from the dopant that are positively charged.

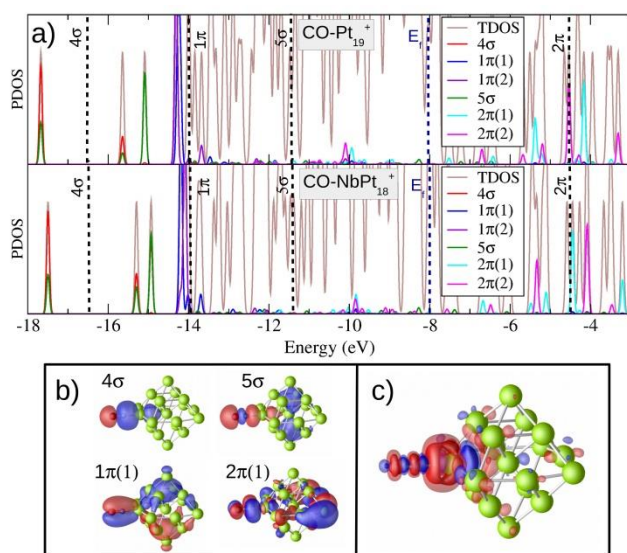


Figure 4. a) Projected densities of states (PDOS) on the CO molecular orbitals (MO) for CO-Pt_{19}^+ and CO-NbPt_{18}^+ . The brown line shows total DOS. Dashed vertical lines indicate the position of free CO MO's. (b) Wave functions of selected CO related states on CO-Pt_{19}^+ . (c) Plot of induced charge density differences for CO-Pt_{19}^+ . Red/blue contours represent regions of charge accumulation/depletion, respectively.

Figure 4 provides an analysis of the cluster–CO bond. There is a strong interaction between the 5σ orbital, which is strongly shifted down in energy, and the Pt d states. In addition, hybridization between the 2π MO and the d states results in levels with partially 2π character below the Fermi energy. Also the CO 1π MOs hybridize with Pt states. The shapes of charge redistributions upon bonding confirm a major role of donation from σ orbitals, which becomes more difficult when the Pt reaction sites are negatively charged.

In summary, a combined mass spectrometric and density functional theory study has shown that a single dopant atom in small cationic Pt clusters alters the interaction strength of the clusters with CO. The magnitude of the effect depends on the

kind of dopant atom, with a significant change in the cluster–CO interaction upon Nb and Mo doping and no or minor influence for Sn and Ag doping. The Nb and Mo dopants occupy highly coordinated positions in the clusters concomitant with a large dopant–Pt charge transfer, thereby affecting the local electronic structure of all Pt atoms including the CO reaction site. This is not the case for Sn and Ag, which take low coordinated positions in the Pt clusters. The higher occupancy of the Pt valence d band in Nb and Mo doped clusters is responsible for the reduced CO adsorption energies, which explains the lower abundances of the cluster– $(\text{CO})_2$ complexes in the experiment.

Several Pt alloy nanoparticles, including PtNb, PtMo, PtSn and PtAg, have been tested in real PEMFCs and show an improved tolerance to CO poisoning. We demonstrated the particular role of intraparticle charge transfer on the CO binding energies in Pt clusters containing a single dopant atom. Since CO binding is a local event, conclusions from this work may be relevant for larger Pt-X alloy nanoparticles that show enhanced CO tolerance and should be considered when developing future fuel cells with better durability.

Acknowledgements

This work is supported by the Research Foundation-Flanders (FWO) and by the KU Leuven Research Council (GOA/14/007). P. Ferrari acknowledges CONICYT for Becas Chile scholarship. The work in Valladolid was supported by MINECO (Grant MAT2014-54378-R) and Junta de Castilla y Leon (Grant VA050U14).

Keywords: CO tolerance • Pt clusters • doped clusters • mass spectrometry • DFT simulation

- [1] X. Zhao, M. Yin, L. Ma, L. Liang, C. Liu, J. Liao, T. Lu and W. Xing, *Energy Environ. Sci.* **2011**, *4*, 2736.
- [2] J. Baschuk, and X. Li, *Int. J. Energy Res.* **2001**, *25*, 695.
- [3] S. Ehteshamia and S. Chan, *Electrochim. Acta* **2003**, *93*, 334.
- [4] Y. Feng, L. Bi, Z. Liu, D. Kong and Z. Yu, *J. Catal.* **2012**, *290*, 18.
- [5] J. Hu, Z. Liu, B. Eichhorn and G. Jackson, *Int. J. Hydrogen Energy*, **2012**, *37*, 11268.
- [6] J. Kim, S. Choi, S. Nam, M. Seo, S. Choi and W. Kim, *Appl. Catal. B- Environ.* **2008**, *82*, 89.
- [7] T. Rocha, F. Ibanhi, F. Colmati, J. Linares, V. Paganin, E. Gonzalez, *J. Appl. Electrochem.* **2013**, *43*, 817.
- [8] J. K. Nørskov, T. Bligaard, J. Rossmeisl and C. H. Christensen, *Nat. Chem.* **2009**, *1*, 37.
- [9] G. Blyholder, *J. Chem. Phys.* **1964**, *68*, 2772.
- [10] N. Dimakis, M. Cowan, G. Hanson and E. S. Smotkin, *J. Phys. Chem. C* **2009**, *113*, 18730.
- [11] M. Liao, C. Cabrera and Y. Ishikawa, *Surf. Sci.* **2000**, *445*, 267.
- [12] H. Schwarz, *Angew. Chem. Int. Ed.* **2015**, *54*, 10090; *Angew. Chem.* **2015**, *127*, 10228.
- [13] S. Zhou, J. Li, M. Schlangen and H. Schwarz, *Acc. Chem. Res.* **2016**, *49*, 494.

- 1 [14] S.M. Lang, I. Fleischer, T.M. Bernhardt, R.N. Barnett and U. Landman, *J.*
2 *Am. Chem. Soc.* **2012**, *134*, 20654.
- 3 [15] D. Justes, R. Mitrić, N. Moore, V. Bonačić-Koutecký and A. Castleman Jr.,
4 *J. Am. Chem. Soc.* **2003**, *125*, 6289.
- 5 [16] S. M. Lang, T. Bernhardt, R. Barnett and U. Landman, *Angew. Chem. Int.*
6 *Ed.* **2010**, *49*, 980; *Angew. Chem* **2010**, *122*, 933.
- 7 [17] V. Kaydashev, E. Janssens and P. Lievens, *Int. J. Mass Spectrom.* **2015**,
8 *379*, 133.
- 9 [18] H. Le, S. M. Lang, J. De Haeck, P. Lievens and E. Janssens, *Phys. Chem.*
10 *Chem. Phys.* **2012**, *14*, 9350.
- 11 [19] E. Janssens, H. Le and P. Lievens, *Chem. Eur. J.* **2015**, *21*, 1.
- 12 [20] J. Mortensen, L. Hansen and K. Jacobsen, *Phys. Rev. B* **2005**, *71*,
13 035109.
- 14 [21] J. Enkovaara et al. *J. Phys.: Condens. Matter* **2010**, *22*, 253202.
- 15 [22] J. Perdew, K. Burke and M. Ernzerhof, *Phys. Rev. Lett.* **1996**, *77*, 3865.
- 16 [23] M. Marques, M. Oliveira and T. Burnus, *Comput. Phys. Commun.* **2012**,
17 *183*, 2272.
- 18 [24] L. Xiao and L. Wang. *J. Chem. Phys.* **2004**, *108*, 8605.
- 19
20
21
22
23
24
25
26
27
28
29
30
31
32
33
34
35
36
37
38
39
40
41
42
43
44
45
46
47
48
49
50
51
52
53
54
55
56
57
58
59
60
61
62
63
64
65